

Analysis of Threshold-Based ToA Estimators in UWB Channels

Invited paper

March 27, 2006

ABSTRACT

In this paper we analyze and compare the performance of matched filter (MF) and energy detector (ED) time-of-arrival estimators based on thresholding in ultra-wide bandwidth (UWB) dense multipath channels. Closed-form expressions for the estimator bias and mean square error (MSE) are derived as a function of signal-to-noise ratio using a unified methodology. A comparison with results based on Monte Carlo simulation confirms the validity of our analytical approach. In addition, results based on experimental measurements in an indoor residential environment are presented as well. Our analysis enables us to determine the threshold value that minimizes the MSE, critical parameter for optimal estimator design. It is shown that the estimation accuracy mainly depends on large estimation errors due to peak ambiguities caused by multipath at the output of the MF or ED and on the fading statistics of the first path. The evaluation of the performance loss faced by ED estimators with respect to those based on MF is also carried out.

1. INTRODUCTION

One of the most attractive capabilities of ultra-wide bandwidth (UWB) technology is accurate positioning capability due to its fine delay resolution [1, 2]. Ranging among two nodes based on the estimation of the first arriving path can be difficult in multipath channels especially under the non-line-of-sight (NLOS) condition in which, the direct path (if it exists) is not always the strongest one and that makes the estimation of the time-of-arrival (ToA) challenging.

In additive white Gaussian noise (AWGN) channels the classical correlation or equivalently, matched filter (MF) estimator is known to be asymptotically efficient since it achieves the Cramér - Rao lower bound (CRLB) for large signal-to-noise ratios (SNR) [3]. On the other hand, energy detector (ED) based estimators are gaining a large interest due to their low complexity implementation at sub-Nyquist sampling rates [4].

In the presence of multipath, or at low SNR, the output of the MF and ED estimators exhibits adjacent peaks with similar height due to noise, multipath, and pulse shape, all of which engender ambiguity in the selection of the correct peak. In this case, the estimation performance is dominated by *large errors* (also called *global errors*) whose magnitude is greater than the width of the transmitted pulse. As a consequence, ToA estimate tends to be biased and the corresponding mean square error (MSE) increases drastically for SNR's below a certain value, a behavior typically known as *thresholding phenomena* [5].

A simple technique to detect the first arriving path in such a harsh propagation environment is to compare the output

of the MF and ED with a threshold which value has to be optimized according to the operating condition (e.g., SNR), as will be shown in the following sections.

The adoption of the threshold-based estimators is attractive because complexity and computational constraints are often critical issues in applications that require low cost battery-powered devices (e.g., in wireless sensor networks or RFID). For these reasons, characterizing the performance for the threshold-based estimator is of considerable importance.

To the best of authors' knowledge, most of previous works evaluate the estimation performance by using asymptotic analysis (large SNR) or by simulations/measurements [6, 7]. Analytical expressions for the bias and MSE of the estimator in the non-asymptotic regions are often difficult to compute. In [8], bounds on the variance of the large errors are derived and the ToA estimation performance is evaluated by simulation, whereas in [4] a semi-analytical approach aided by simulations is proposed.

In this paper a unified performance evaluation of both MF and ED threshold-based ToA estimators is addressed for UWB signals in indoor residential environment. In particular, the bias and the MSE of the estimation are evaluated as a function of SNR for various operating conditions, thereby overcoming the limitation of conventional asymptotic analysis valid only for high SNR. The validity of the methodology is confirmed by comparing the analytical results with the results based on Monte Carlo simulations as well as results from experimental measurements which showing good agreement. The evaluation of the performance loss faced by ED estimators with respect to those based on MF is carried out to understand the tradeoff for a lower implementation complexity.

2. TOA THRESHOLD-BASED ESTIMATORS

We consider a multipath scenario where a single pulse $p(t)$, with duration T_p and energy E_p , is transmitted.¹ The received signal $r(t)$ after the ideal bandpass zonal filter (BPZF), with bandwidth W and center frequency f_c around the signal band to eliminate the out-of-band noise, can be written as [9]

$$r(t) = \sum_{l=1}^L \alpha_l p(t - \tau_l) + n(t), \quad (1)$$

where L is the maximum number of multipath components, $n(t)$ is AWGN with zero mean and two-sided power spectral density $N_0/2$ within the BPZF bandwidth W , whereas $\{\tau_2, \tau_3, \dots, \tau_L, \alpha_1, \alpha_2, \dots, \alpha_L\}$ is a set of nuisance parameters composed of the path gains α_l 's and delays τ_l 's. The channel

¹For simplicity we consider single pulse transmission. The extension to multiple pulse transmissions is straightforward.

is modeled as tapped delay line where $\tau_l = \tau_1 + \Delta \cdot (l - 1)$, with $\Delta \approx T_p$ is the width of a resolvable time slot and $\Delta \cdot (L - 1)$ is the channel delay spread [10]. According to [9, 10], the complex path gain α_l in (1) can be written in general as $\alpha_l = b_l \beta_l e^{j\phi_l}$ with β_l and ϕ_l denoting the paths' amplitude and phase respectively, and b_l being a random variable (r.v.) taking the values 1 (path present) and 0 (path absent) with probability p_b and $1 - p_b$, respectively. In this way both channel models with random and fixed path delays (by setting $p_b = 1$ where the path is always present) can be approximated. We consider a resolvable multipath channel, i.e., $|\tau_i - \tau_j| \geq \Delta$ for each $i \neq j$. When the multipath is not resolvable, the following analysis gives a lower bound on the achievable performance.

We are interested in the estimation of the ToA of the first arriving path where $\tau = \tau_1$, by observing the received signal $r(t)$ over the interval $[0, T)$. In the absence of multipath, the observation of the instant t_1 corresponding to the maximum peak at the output of the MF and yields a maximum likelihood estimate, which is asymptotically efficient, i.e., for high SNR the estimated ToA $\hat{\tau}$ becomes unbiased with variance given by the CRLB [3]

$$\text{CRLB} = \frac{N_0/2}{E_p \alpha_1^2 \kappa^2}, \quad (2)$$

where the parameter $\kappa^2 \triangleq \int_{-\infty}^{\infty} f^2 |P(f)|^2 df / E_p$ represents the second moment of the spectrum $P(f)$ of $p(t)$.

In a multipath environment, the presence of noise and fading can strongly affect the ToA estimation. In the MF based scheme, one possible procedure is a two-stage process. First, detect the portion of the observation interval in which the first path is located by comparing the output of a rectifier device (or, equivalently, a square-law device inserted after the MF to remove sign ambiguity of the path amplitude) to a fixed threshold λ [3]. Then make a fine delay estimation by peak searching.² The output of this maxima search, subtracted by the MF delay T_d , is taken as the estimate of the ToA τ . A second procedure is to consider an ED which output is compared to the threshold λ [4]. The first threshold crossing event is taken as the estimate of the ToA. In both cases the performance of the detection process, hence of the ToA estimation, depends on the choice of the threshold λ which plays important role in the optimum design of threshold-based ToA estimators.

3. EVALUATION OF THE ESTIMATION BIAS AND MSE

We subdivide the observation interval into $N = T/\Delta$ slots of length Δ . In the following analysis, we approximate noise samples taken in different slots to be statistically independent. Note that the interval $[0, \tau - \Delta/2]$, corresponding to the first $N_f = \tau/\Delta$ slots, contains only noise signal (*noise region*), whereas the interval $[\tau - \Delta/2, T]$, corresponding to the remaining $N_m = N - N_f$ slots, may contain, in addition to the noise, dense multipath echoes (*multipath region*).³ We number the slots starting from that containing τ , so that slots 1, 2,

²If particular complexity constraints are present, the refinement stage can be skipped. In this case our analysis will provide a lower bound on the achievable performance.

³The parameters N and N_f are approximated as the integer closest to T/Δ and τ/Δ , respectively.

3, ..., N_m correspond to the multipath region, whereas slots 0, $-1, -2, \dots, -N_f + 1$ correspond to the noise region. The true ToA τ is contained in the slot 1.

3.1 Characterization of MF Estimator Decision Variable

In the presence of multipath, the rectifier device output $v^{(\text{MF})}(t)$ can be written, using (1), as⁴

$$v^{(\text{MF})}(t) = \left| \sum_{l=1}^L \alpha_l \Phi_p(t - \tau_l) + z(t) \right|, \quad (3)$$

where $\Phi_p(\tau)$ is the autocorrelation function of the pulse $p(t)$ and $z(t)$ is the colored Gaussian noise at the output of the MF with autocorrelation function $\Phi_z(\tau) = N_0 \Phi_p(\tau)/2$. Note that $\Phi_z(\tau) \simeq 0$ for $|\tau| \geq T_p$, hence noise samples taken at instants more than $2T_p$ apart are independent.

It is convenient to define

$$v_l^{(\text{MF})} \triangleq v^{(\text{MF})}(t_l) = |\alpha_l \Phi_p(0) + z_l| \quad 1 \leq l \leq L \quad (4)$$

as the values of $v(t)$ at $t_l = \tau_l$, where $z_l \triangleq z(t_l)$, and

$$q_k^{(\text{MF})} \triangleq \begin{cases} \mathbb{P} \{ v_k^{(\text{MF})} > \lambda \} & 1 \leq k \leq L \\ \mathbb{P} \{ |z(t)| > \lambda \} & \text{otherwise,} \end{cases} \quad (5)$$

which is the probability that the modulo of the MF output exceeds the threshold λ at time τ_k (when $1 \leq k \leq L$) and the probability that only noise components overcome the threshold (when $k = \dots - 2, -1, 0, L+1, L+2, \dots$). The latter is given by

$$q_o^{(\text{MF})} \triangleq q_k^{(\text{MF})} = \mathbb{P} \{ |z(t)| > \lambda \} = 2Q \left(\frac{\lambda}{\sigma} \right), \quad (6)$$

where $\sigma^2 = \Phi_p(0)N_0/2 = E_p N_0/2$ and $Q(\cdot)$ is the Gaussian probability integral.

We also define the following ratios: the SNR related to the (average) energy of the first arriving path $\text{SNR} \triangleq E_p \mathbb{E} \{ \alpha_1^2 \} / N_0$ and the threshold-to-noise ratio (TNR) $\text{TNR} \triangleq \lambda / N_0$. Without loss of generality we consider the normalization $\mathbb{E} \{ \alpha_1^2 \} = 1$.

3.2 Characterization of ED Estimator Decision Variable

For the ED estimator, the sampled outputs at each time slot can be written as [4]

$$v_k^{(\text{ED})} = \int_{(k-1)\Delta + \tau - \Delta/2}^{(k-1)\Delta + \tau + \Delta/2} |r(t)|^2 dt. \quad (7)$$

Also in this case we define

$$q_k^{(\text{ED})} \triangleq \mathbb{P} \{ v_k^{(\text{ED})} > \lambda \} \quad (8)$$

where in the noise region, i.e., for $k = \dots - 2, -1, 0, L+1, L+2, \dots$, $v_k^{(\text{ED})}$ have a centralized Chi-square distribution with $M = 2\tilde{W}\Delta$ degree of freedom [4, 11]. We have

⁴For the purpose of the analysis, without loss of generality, we can set $T_d = 0$.

$$q_0^{(\text{ED})} \triangleq q_k^{(\text{ED})} = \exp(-\text{TNR}) \sum_{i=0}^{M/2-1} \frac{\text{TNR}^i}{i!}. \quad (9)$$

Since noise samples taken in different slots are statistically independent, v_k defined in (4) and (7) are statistically independent. In the following for notation convenience, $q_k^{(\text{ED})}$ and $q_k^{(\text{MF})}$ will be denoted with q_k .

3.3 Analytical Methodology Formulation

Armed with the definitions above, we now proceed with the formulation to obtain the bias and MSE of the threshold-based ToA estimator. Based on the Total Probability Theorem, the bias and MSE of the ToA estimate can be written respectively as [12, 13]

$$\mu = \mathbb{E}\{\hat{\tau} - \tau\} = \sum_{n=-N_f+1}^{N_m} P_n \cdot \mathbb{E}\{(\hat{\tau} - \tau) | \text{slot } n\} + P_{\text{miss}} \cdot \mathbb{E}\{(\hat{\tau} - \tau) | \text{miss}\} \quad (10)$$

$$\text{MSE} = \mathbb{E}\{(\hat{\tau} - \tau)^2\} = \sum_{n=-N_f+1}^{N_m} P_n \cdot \mathbb{E}\{(\hat{\tau} - \tau)^2 | \text{slot } n\} + P_{\text{miss}} \cdot \mathbb{E}\{(\hat{\tau} - \tau)^2 | \text{miss}\} \quad (11)$$

where P_n is the probability of the first level crossing occurrence in slot n (responsible for large errors if $n \neq 1$) and P_{miss} is the probability of the “no level crossing” event and $\mathbb{E}\{\cdot\}$ denotes the statistical expectation. The terms $\mathbb{E}\{(\hat{\tau} - \tau) | \text{slot } n\} = (n-1)\Delta$ and $\mathbb{E}\{(\hat{\tau} - \tau)^2 | \text{slot } n\} = [n(n-2) + 13/12]\Delta^2$ are, respectively, the bias and MSE conditioned on the first level crossing occurrence in slot n . We assumed that the estimation error is uniformly distributed in the n^{th} slot.

When the MF estimator is adopted, to obtain good asymptotical behavior, the bias and MSE, conditioned on the threshold crossing in slot 1, can be replaced by the asymptotic performance of the ML estimator, i.e., $\mathbb{E}\{(\hat{\tau} - \tau) | \text{slot } 1\} = 0$ and $\mathbb{E}\{(\hat{\tau} - \tau)^2 | \text{slot } 1\} = \text{CRLB}$ respectively [3], which tends to zero as SNR increases. Using the ED estimator a floor on the MSE conditioned on the first level crossing event in slot 1, is present, i.e., $\mathbb{E}\{(\hat{\tau} - \tau)^2 | \text{slot } 1\} = \Delta^2/12$, regardless of the SNR.

The terms $\mathbb{E}\{(\hat{\tau} - \tau) | \text{miss}\}$ and $\mathbb{E}\{(\hat{\tau} - \tau)^2 | \text{miss}\}$ are related to the bias and MSE conditioned to the “no level crossing” event according to the peak miss policy adopted. One possibility is to choose $\hat{\tau}^{\text{miss}} = T/2$, i.e., in the middle of the observation interval.⁵ In this case, it is $\mathbb{E}\{(\hat{\tau} - \tau) | \text{miss}\} = \hat{\tau}^{\text{miss}} - \tau$, and $\mathbb{E}\{(\hat{\tau} - \tau)^2 | \text{miss}\} = (\hat{\tau}^{\text{miss}} - \tau)^2$.

Since the noise samples in different slots are statistically independent, the evaluation of probabilities P_n is considerably simplified. In the noise region we have

$$P_n = q_0 (1 - q_0)^{N_f + n - 1}, \quad (12)$$

⁵Another possibility is to retry with a lower threshold until a level crossing occurs or consider the maximum peak.

for $-N_f < n \leq 0$. This corresponds to the probability of a level crossing in slot n , preceded by no level crossing in $N_f + n - 1$ slots. In the multipath region, assuming independent fading among different paths, we have

$$P_n = q_n (1 - q_0)^{N_f} \prod_{k=1}^{n-1} (1 - q_k), \quad (13)$$

for $0 < n \leq N_m$. This corresponds to the probability that a level crossing at time index n is preceded by no level crossing in the N_f slots composing the noise region and in the first $n - 1$ slots in the multipath region. The probability of no level crossing is simply the probability that none of the peaks cross the threshold, i.e.,

$$P_{\text{miss}} = (1 - q_0)^{N_f} \cdot \prod_{k=1}^{N_m} (1 - q_k). \quad (14)$$

3.4 Evaluation of Probabilities q_k

In order to evaluate (12), (13) and (14) (and ultimately the bias and the MSE), we must provide an expression for the probabilities q_k ($k = 1, 2, \dots, L$) defined in (5) and (8) through the adoption of a suitable channel model for the paths' amplitudes. The probabilities for other values of k are given by q_0 defined in (6) and (9). According to [9], the k^{th} path amplitude β_k is a Nakagami- m r.v. with parameters m_k (fading parameter, $m_k \geq 0.5$) and $\mathbb{E}\{\beta_k^2\} = \Lambda_k$. The phase ϕ_k can take the values $\{0, \pi\}$ with equal probability.

The evaluation of q_k for $k = \{1, 2, \dots, L\}$ when the MF estimator is adopted is presented in [12, 13]. In the ED estimator case, we derive an expression by extending the semi-analytical result in [4].

Following the sampling approach similarly as done in [11], the r.v. v_k , conditioned to the path amplitude β_k , has a centralized Chi-square distribution with $M = 2W\Delta$ degree of freedom if $b_k = 0$ (path absent). When $b_k = 1$ (path present), v_k has a non-centralized Chi-square distribution with central parameter $E_p \beta_k^2$ which represents the signal energy in the slot k . The probability $q_k |_{\beta_k}$ conditioned on the path amplitude β_k is then given by

$$q_k |_{\beta_k} = \mathbb{P}\left\{v_k > \lambda \middle| \beta_k\right\} = (1 - p_b) q_0 + p_b Q_{M/2}\left(\sqrt{2 \text{SNR} \beta_k^2}, \sqrt{2 \text{TNR}}\right), \quad (15)$$

where $Q_m(\cdot, \cdot)$ denotes the Marcum-Q function. By averaging over the path's amplitude β_k we obtain the final expression for q_k

$$q_k = (1 - p_b) q_0 + p_b \mathbb{E}\left\{Q_{M/2}\left(\sqrt{2 \text{SNR} \beta_k^2}, \sqrt{2 \text{TNR}}\right)\right\} = q_0 + p_b \sum_{h=M/2}^{\infty} e^{-\text{TNR}} \frac{\text{TNR}^h}{h!} \left[1 - \sum_{i=0}^{h-M/2} \frac{\Gamma(m_k + i)}{\Gamma(m_k) i!}\right] \times \left(\frac{1}{1 + \text{SNR} \Lambda_k / m_k}\right)^{m_k} \left(\frac{\text{SNR} \Lambda_k / m_k}{1 + \text{SNR} \Lambda_k / m_k}\right)^i, \quad (16)$$

where $\Gamma(\cdot)$ is the Euler gamma function.

4. MEASUREMENTS AND DATA ANALYSIS

4.1 Measurement Setup

In order to evaluate the performance of the threshold-based ToA estimator under realistic channel condition, an UWB experiment was performed in the indoor residential environment. Measurements were conducted in the frequency-domain in which the channel transfer function (CTF), $H(f)$ was measured and stored. The measurement system consists of a vector network analyzer (VNA), a 30 dB gain wideband power amplifier, a 32 dB gain low noise amplifier, an attenuator and a pair of vertically polarized wideband planar dipole antennas (see the overview of the measurement setup in [14]). During the measurements, all antennas had the same height and the VNA was set to transmit 1601 continuous waves tones uniformly distributed over the 3 – 10 GHz frequency range (i.e., with center frequency of 6.5 GHz), which results in a frequency step of 4.375 MHz. This frequency resolution gives maximum excess delay of about 229.6 ns and maximum distance range of approximately 68.6 m. The 7 GHz bandwidth gives a temporal resolution of 142.9 ps. By setting the intermediate frequency bandwidth of the VNA to 3 kHz, the sweeping time is automatically adjusted to sweep the 7 GHz bandwidth in 800 ms. Thus, the maximum measurable Doppler spread would be 1.25 Hz (i.e., $1/800$ ms). The VNA measures the S-parameter of the UWB channel at each receiving antenna which essentially corresponds to the CTF. For more details of the measurement campaign, please refer to [14, 15].

4.2 Measurement Procedure and Environments

Field measurements have been conducted in various types of high-rise apartment that have different sizes, layouts and structures. In each apartment, the transmitter (TX) was placed at a fixed position (i.e., in the center of the living room), while the receiver (RX) was moved throughout the apartment around 8 – 10 different positions with TX-RX separation ranging from 1 – 20 m. We refer this different RX positions as *local points* [14, 15]. Both LOS and NLOS scenarios were considered which include “within-room” and “room-to-room” propagation conditions where all doors and windows were closed during the measurements. Two levels of measurements were performed. Firstly, the random placements of RX throughout the apartment and secondly, the RX was moved 25 times around each local point. These 25 spatial measurements were arranged over a 5×5 square grid with 15 cm spacing between adjacent points. Each point on the grid is referred as a *spatial point*. The height of both TX and RX were fixed at 1.25 m from the floor and from the ceiling so that they are in the same horizontal plane. During the measurements, both TX and RX antennas and the channel were kept stationary by ensuring there was no movement in the physical surrounding environment. However, in order to confirm the time-invariant nature of the channel and for statistical analysis reliability, at each spatial point, 30 time-snapshots of the complex CTFs were recorded. The measured CTFs were showed in [15] with no perceptible differences. Thus, we can conclude that the channel was static over the measured time frames.

4.3 Data Analysis

By assuming that the channel is quasi-static, averaging is carried out over the time-domain for each block of 30 time-snapshots of CTFs measured at each spatial point. This assumption is justified since no movement was allowed during the measurements. The resultant time-averaged CTFs are post-processed by frequency domain Hamming windowing in order to reduce the leakage problem prior to transformation into the time domain. The windowed time-averaged CTFs were transformed into the channel impulse responses (CIRs), $h(\tau)$ through the real passband inverse Fourier transform (IFT). The spectrum is obtained by first zero-padding the complex CTF down to DC, and then flipping the complex conjugate of the positive spectrum to the negative frequencies to give the complete symmetric spectrum. This guarantees the IFT would be real. A detailed comparison between these two analysis techniques is reported in [14]. The initial delay for each of the transmission links was eliminated from the CIR in order to remove the propagation effect due to the TX-RX separation. This adjustment can be done based by setting the ToA of the first detectable path in each CIR equal to zero. Thus, this enabling various data sets from each of the TX-RX combinations to be aligned and compared. For the LOS data, the first arrival path is identified within 10 dB and 10 ns from the peak power, while for the NLOS data, first arrival path is identified within 10 dB and 50 ns from the peak power. A cutoff threshold of 30 dB below the strongest path was applied to the CIR so that any paths below this threshold are set to zero. By setting such a strict threshold level, unwanted noise spikes can be eliminated and can ensure that only the effective paths are used by the threshold-based ToA estimator.

Fig. 1 depicts the typical small-scale averaged power delay profiles (SSA-PDP) under the NLOS condition obtained by averaging 25 PDPs at each local point. We see clearly that the first arriving path is strongly attenuated, and the maximum in the SSA-PDP occurs only after about 20 ns. These characteristics of UWB channels are significant for precision ranging and localization applications especially to the design of threshold-based ToA estimator, since the technique requires the detection of the *first* arriving path and not the strongest path. Detection of such a weak component in a noisy environment can be quite challenging and will be shown was taken into account in our proposed analytical model.

5. NUMERICAL RESULTS AND DISCUSSION

5.1 Validation of the Analytical Methodology

In this section, we provide numerical illustrations using analytical results obtained in previous sections. We consider a dense multipath channel with exponential power delay profile where the average path power gains are given by $\Lambda_l = e^{-\Delta(l-1)/\varepsilon}$ for $l = 1, 2, \dots, L$ [9]. The parameter ε describes the multipath spread of the channel. As in [16], we choose $\Delta = 2$ ns, $L = 32$, $\varepsilon = 6$ ns, $p_b = 1$ and $m_l = 2$ for our numerical examples.

Next we evaluate the bias and root MSE, $\text{RMSE} = \sqrt{\text{MSE}}$, of the estimation error of our proposed threshold-based ToA estimator for $\tau = 20$ ns, $T = 100$ ns, $W = 7$ GHz and the second derivative Gaussian monocycle pulse with $T_p = 1$ ns ($\kappa^2 = 10\pi 10^{18} \text{ s}^{-2}$).

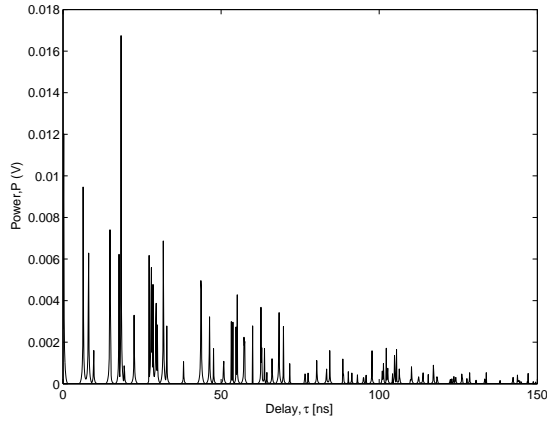


Figure 1: Example of channel power delay profile under NLOS condition

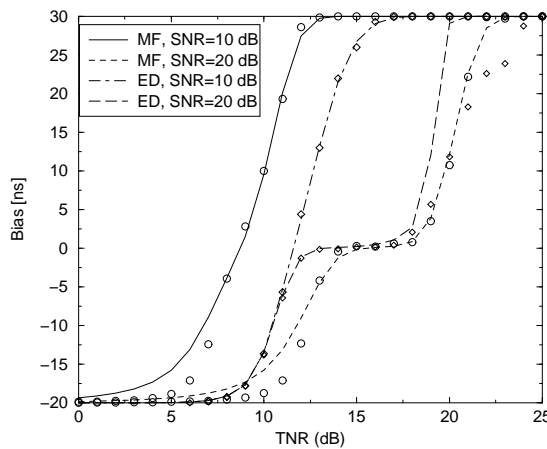


Figure 2: Estimator bias versus TNR (dB) for different SNR values. Comparison between analytical and Monte-Carlo simulation results.

Figs. 2 and 3 show the bias and the RMSE as a function of the TNR for different values of SNR. It can be seen that for small values of TNR the estimated ToA tends to be negative due to false alarms in the noise region, whereas large TNRs lead to positive bias in the estimate, due to the presence of multipath. For very large values of TNR, the bias is related to the miss policy adopted when no level crossing is present. In this case $\mathbb{E}\{(\hat{\tau} - \tau)|\text{miss}\} = T/2 - \tau = 30$ ns. There is an optimum value of the threshold, depending on the SNR, which makes the estimation unbiased and minimizes the MSE. Figs. 2 and 3 also report the Monte Carlo simulation results (points) for comparison. It can be noted that our analytical results are in good agreement with simulation results for a wide range of SNRs.

Fig. 4 shows the MSE as a function of SNR obtained by considering the optimal value of λ that minimizes MSE for each SNR. In this figure, we consider the cases where the first path is subjected to Nakagami fading with $m_1 = 2$ and $m_1 = 10$, respectively. The former case is typical for NLOS situations, whereas the latter case is typical for line-of-sight (LOS) situations with essentially no fading. The results are compared to the CRLB. As can be seen in the figure, at high SNR, the ED performance shows a floor equal to

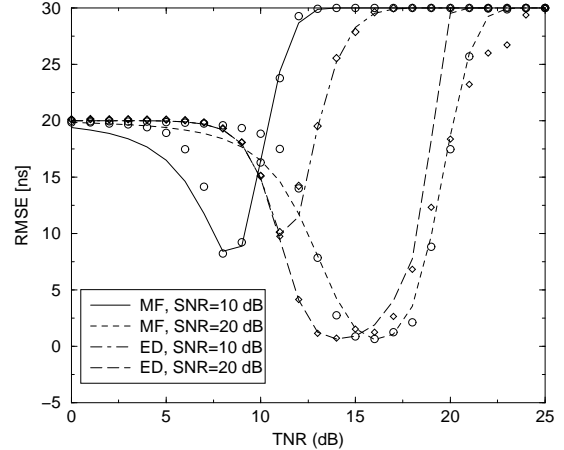


Figure 3: RMSE versus TNR (dB) for different SNR values. Comparison between analytical and Monte Carlo simulation results.

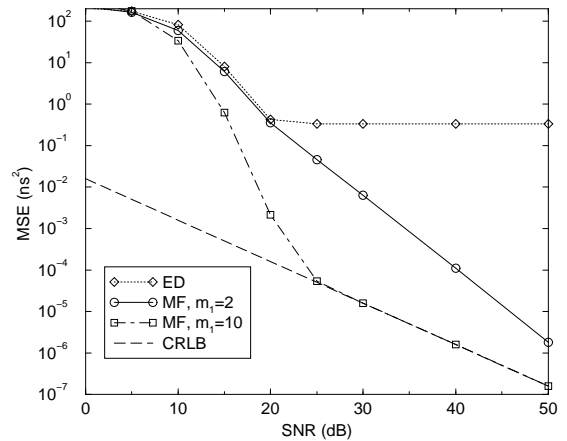


Figure 4: MSE versus the SNR using optimum values of λ . Comparison with the CRLB.

$\Delta^2/12$, whereas the MF performance tends to the CRLB with a behavior depending on the fading of the first path. In the presence of severe fading in the NLOS case, the ToA estimator performance tends slowly to the CRLB only for large values of SNR due to large errors and fading. For low SNR the received signal is highly unreliable and the ToA estimation error is on the order of the observation interval width. In the transition region the performance is far from that predicted by the CRLB, i.e., it is dominated by large errors. When the first path is subjected to small fading in the LOS case, the convergence to the CRLB is faster despite the presence of the multipath components.

5.2 Comparison with Measurement Data

We now compare the performance of the MF and the ED with experimental data obtained from a measurement campaign described in the previous section. Measurement data obtained from Apartment 1 when RX is located at position 3, and 7 (see the measurement plan in [14]), which represents SNR at 14 and 21 dB, respectively, are used for the performance comparison. The average distance between the TX

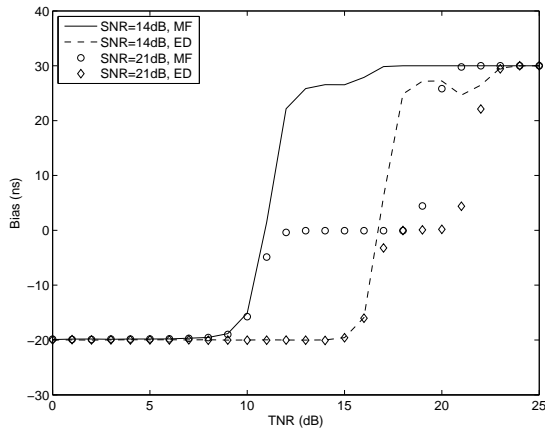


Figure 5: Estimator bias versus TNR (dB) for different SNR values using experimental data.

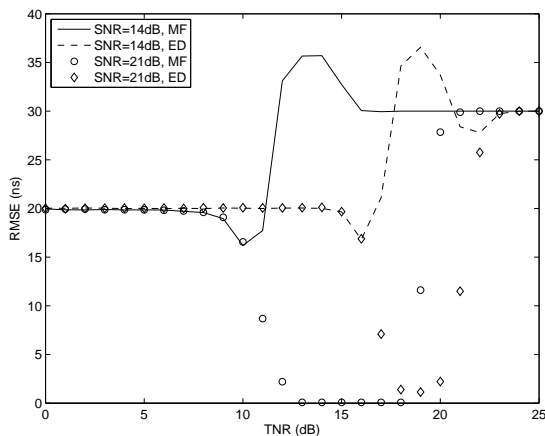


Figure 6: RMSE versus TNR (dB) for different SNR values using experimental data.

and the RX is 5 – 6 m. The impulse shape $p(t)$ is obtained from the reference CIR, $h_{\text{ref}}(\tau)$ measured at 1.3 m under the LOS condition and the true ToA in the simulation is set to $\tau = 20$ ns. Figs. 5 and 6 show the bias and RMSE of the estimation error, respectively, versus the TNR in two different conditions, SNR= 14 and 21 dB for both MF and ED cases. Under the low SNR (i.e., 14 dB), ED suffers significant performance losses where the TNR requires extra 5 dB in order to achieve the similar performance as the MF. On the other hand, under the high SNR (i.e., 21 dB) the performance loss is not that significant. This result implies that ED based receiver is more suitable to be deployed for short-range applications when SNR is relatively high while for longer range applications with low SNR, MF based receiver is desirable in order to achieve a higher ranging accuracy.

6. CONCLUSIONS

Threshold-based ToA estimator performance using MF and ED are characterized in UWB channels. In particular, expressions for the estimators bias and MSE are derived for a wide range of SNRs, thus overcoming the limitation of classical asymptotic analysis valid only for high SNR. Results show that the peak selection ambiguity at the MF or ED device

output is dominant in the presence of multipath and the first arrival path is subjected to severe fading, which is typical of NLOS situations. This leads to large estimation errors resulting in considerable performance degradation when compared to the CRLB, except for extremely high SNRs. A comparison of our analytical results with the results based on simulations confirms the validity of our approach. Based on our analysis, good estimators can be designed by determining the threshold value that optimizes the performance without the need for time-consuming simulations. The performance of the MF and ED ToA estimators is also compared by considering real measurements taken in typical indoor residential environment.

REFERENCES

- [1] R. J. Fontana and S. J. Gunderson, "Ultra-wideband precision asset location system," *Proc. Conf. on Ultra Wideband Sys. and Technol.*, vol. 21, no. 1, pp. 147–150, May 2002.
- [2] S. Gezici, Z. Tian, G. B. Giannakis, H. Kobayashi, A. Molisch, H. V. Poor, and Z. Sahinoglu, "Localization via ultra-wideband radios," *IEEE Signal Processing Magazine*, vol. 22, no. 4, pp. 70–84, Jul 2005.
- [3] H. L. V. Trees, *Detection, Estimation, and Modulation Theory. Part I*, 2nd ed. New York, NY: John Wiley and Son, 2001.
- [4] I. Guvenc and Z. Sahinoglu, "Threshold-based TOA estimation for impulse radio UWB systems," in *Proc. of the IEEE International Conference on Ultra-Wideband, ICU2005*, Zurich, Switzerland, 2005, pp. 420–425.
- [5] J. P. Iannello, "Time delay estimation via cross-correlation in the presence of large estimation errors," *IEEE Trans. Acoust., Speech, Signal Processing*, vol. ASSP-30, no. 6, pp. 998–1003, Dec. 1982.
- [6] J. Zhang, R. A. Kennedy, and T. D. Abhayapala, "Cramer-Rao lower bounds for the time delay estimation of UWB signals," in *IEEE Proc. International Communication Conference, ICC 2004*, Paris, France, May 2004, pp. 3424–3428.
- [7] Z. N. Low, J. H. Cheong, C. L. Law, W. T. Ng, and Y. J. Lee, "Pulse detection algorithm for Line-of-Sight (LOS) UWB ranging applications," *IEEE Antennas Wireless Propagat. Lett.*, vol. 4, pp. 63–67, 2005.
- [8] J. Lee and S. Yoo, "Large error performance of UWB ranging," in *Proc. of the IEEE International Conference on Ultra-Wideband, ICU2005*, Zurich, Switzerland, 2005, pp. 308–313.
- [9] D. Cassioli, M. Z. Win, and A. F. Molisch, "The ultra-wide bandwidth indoor channel: from statistical model to simulations," *IEEE J. Select. Areas Commun.*, vol. 20, no. 6, pp. 1247–1257, Aug. 2002.
- [10] Y.-L. Chao and R. A. Scholtz, "Ultra-wideband transmitted reference systems," *IEEE Trans. Veh. Technol.*, vol. 54, no. 5, pp. 1556–1569, Sept. 2005.
- [11] T. Q. S. Quek and M. Z. Win, "Analysis of UWB transmitted-reference communication systems in dense multipath channels," *IEEE J. Select. Areas Commun.*, vol. 23, no. 9, pp. 1863–1874, Sept. 2005.
- [12] D. Dardari and M. Z. Win, "Threshold-based time-of-arrival estimators in UWB dense multipath channels,"

IEEE Trans. Commun., 2005, submitted for publication.

- [13] —, “Threshold-based time-of-arrival estimators in UWB dense multipath channels,” in *Proc. IEEE Int. Conf. on Commun.*, Istanbul, TURKEY, June 2006.
- [14] C.-C. Chong and S. K. Yong, “A generic statistical-based UWB channel model for high-rise apartments,” *IEEE Trans. Antennas Propagat.*, vol. 53, no. 8, pp. 2389–2399, Aug. 2005.
- [15] C.-C. Chong, Y.-E. Kim, S. K. Yong, and S.-S. Lee, “Statistical characterization of the UWB propagation channel in indoor residential environment,” *Wireless Communications and Mobile Computing, Wiley InterScience*, vol. 5, no. 5, pp. 503–512, Aug. 2005.
- [16] A. Giorgetti, M. Chiani, and M. Z. Win, “Ultrawide bandwidth Rake reception in the presence of narrow-band interference,” in *Proc. IEEE Semiannual Veh. Technol. Conf.*, vol. 3, Milan, ITALY, May 2004, pp. 1659–1663.